Rainbow imaging of 3-D microbubble distribution clustered inside a turbulent boundary layer

Yuichi Murai[1,*], Daichi Saitoh[1], Hyun Jin Park[1], Yuji Tasaka[1]
1: Laboratory for Flow Control, Faculty of Engineering, Hokkaido University, Japan
* Correspondent author: murai@eng.hokudai.ac.jp

Keywords: Color imaging, Drag reduction, Turbulent boundary layer, Microbubbles

ABSTRACT

Microbubbles dispersed in a turbulent boundary layer spatially developing along a flat plate is investigated experimentally. The aim of study is to find out visually how microbubbles interact with turbulent eddies to achieve frictional drag reduction on a wall. For stream Reynolds number up to 3×10^4, microbubble suspended at Stokes number smaller than 10^{-3} is measured. Stream-wise vortices in the boundary layer were visualized by flake optics, of which spacing expands with injection of microbubbles. 3-D microbubble distributions were measured by a color-coded volumetric illumination applied to the boundary layer. The result showed preferentially accumulated microbubble clouds to low-speed streaks close to viscous sublayer and to hair-pin vortices in the buffer layer.

1. Introduction

Introduction Injection of microbubbles can greatly reduce the frictional drag along a solid wall in turbulent flow states. This is a known fact since the paper by McCormick and Bhattacharyya (1973). There were reports trying to explain the mechanism of the drag reduction in 1980s with a mathematical model of turbulent boundary layer (Legner, 1984; Marie, 1987). However, it came to an understanding that it should be elucidated as two-phase flow having significant slip between two phases. This propelled experimental research in 1990s (Merkle and Deutsch, 1992; Kato et al., 1999; Kodama et al., 2000; Moriguchi and Kato, 2002). Most of these experiments used milli-meter or sub-millimeter sized bubbles, smaller than the boundary layer thickness. For these bubbles, turbulent shear stress is often rather enhanced due to complex deformation of bubbles that promote momentum transfer inside the boundary layer. In 2000-2015, deformability of bubbles was focused by the experimental investigators as a major factor contributing to drag reduction (Kitagawa et al., 2005; van Gils et al., 2013; Tasaka et al., 2015). For real microbubbles that keeps spherical shape, capillary number is sufficiently small because of strong surface tension. Question is whether bubble deformation contributes to the drag reduction. Numerical researchers found an effect of microbubble accumulation into individual vortex cores, which alters the size and the location of the vortices (Ferrante and Elghobashi, 2004). However, point-source approximation of the microbubbles did not simulate volumetric clustering effect of microbubbles. In experimental approaches, most of the papers (Serizawa et al., 2005; Gutierrez-Torres et al., 2008; Hara et al., 2011; Shatat et al., 2009) reported significant effect of such real microbubbles on drag reduction even by the volume fraction lower than 1%. A key to explain the mechanism is to clarify where and how such microbubbles are accumulated and modify the local turbulent eddies.

In our experimental study, we have employed a method to visualize 3-D distribution of microbubbles. The method relies on volumetric illumination of microbubbles using a rainbow-type color-coded light applied in a wall proximity. The optical set-up requires only a single camera, allowing effective measurement volume to be kept large enough. A similar technique was reported for tracer particles as the 3-D particle tracking velocimetry (Watamura et al., 2013; Xiong et al., 2019; Noto et al., 2021; Park et al., 2021; Noto et al., 2023). Our case is to apply the technique for microbubbles which scatters light in a way different from solid particles. A basic principle of the method was reported by the authors previously (Park et al., 2018). In the present paper, we report on the application of the technique combined with PIV analysis for elucidating the inner structure of the turbulent boundary layer altered by the present of microbubbles.

2. Experimental Method

A schematic diagram of experimental facility is shown in **Fig. 1**. It consists of an open water horizontal channel of 3,500 mm in total length and a test plate set vertically in the downstream region of the channel. The recirculation unit is constructed by a pump, a flowmeter, and a bubble separating reservoir tank. The open channel around the test plate is made of transparent acrylic resin for all the three sides to allow various optical visualizations.

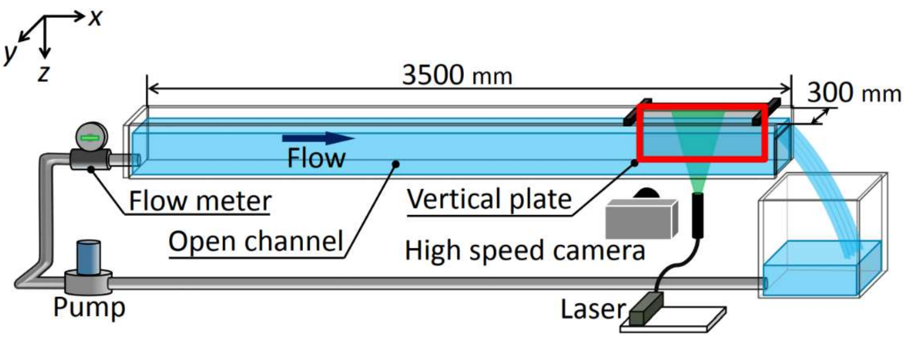

Figure 1 Open channel for visualizing microbubble-laden flat-plate turbulent boundary layer.

We apply the rainbow illumination to turbulent boundary layer along the test plate in the open channel as illustrated in **Fig. 2a**. Hue value is changed linearly to the distance from the plate surface on the order of red, magenta, blue, cyan, green, yellow and returning to red. Width of the rainbow part is set 12 mm, which is about the boundary layer thickness of the flow. In outer layer at y > 12 mm, red monochromatic light is continuously projected so that microbubbles bursting off the boundary layer is identified as red color. An original snapshot of microbubbles image is shown in **Fig. 2b**. Cyan dots in the image correspond to microbubbles flowing in wall proximity at y < 3 mm while magenta dots are microbubbles accumulated in turbulent eddies at 4 mm < y < 7 mm. Yellow spots are microbubbles being ejected toward outer layer at 9 mm < y < 12 mm. The exact computation of the depth coordinate of individual microbubbles is performed from measured hue information after opto-geometrical calibration.

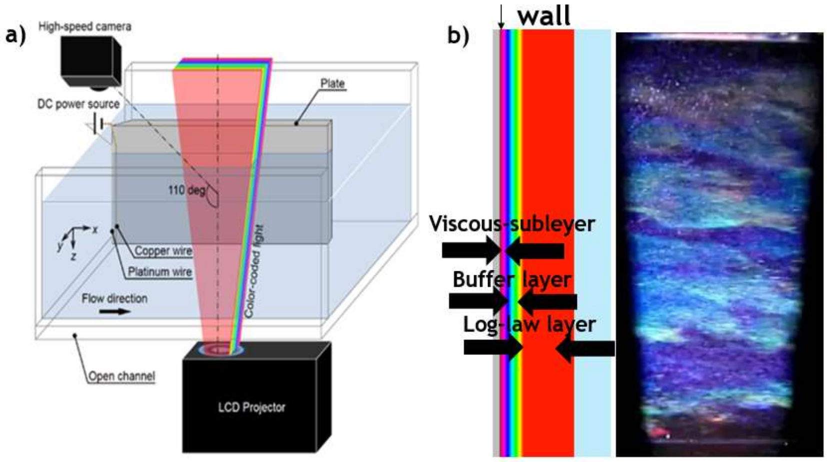

Figure 2 Microbubble visualization by means of color-coded volumetric illumination. (a) Tangential projection of color-coded light and (b) the color coding of the boundary layer, by which microbubbles reflect corresponding colors.

3. Experimental Results

3-1. Microbubble distribution

By sampling a vertical segment from the high-speed video camera movie, timeline blow up images are generated as shown in Fig. 3. In each panel, the horizontal axis indicates time within 5 seconds.

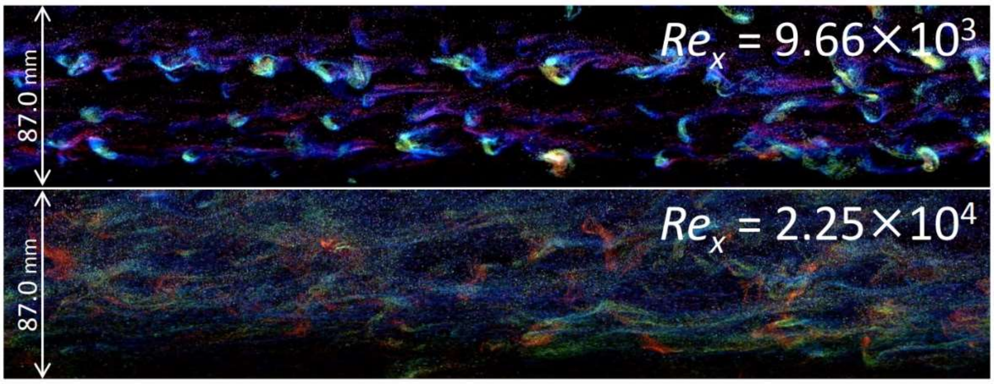

Figure 3 Time-line blow up image of coloured microbubbles. Top figure is the case of Rex = 9,660 taken in the upstream part of the plate. Bottom figure is that of Rex = 22,500 taken in the downstream part.

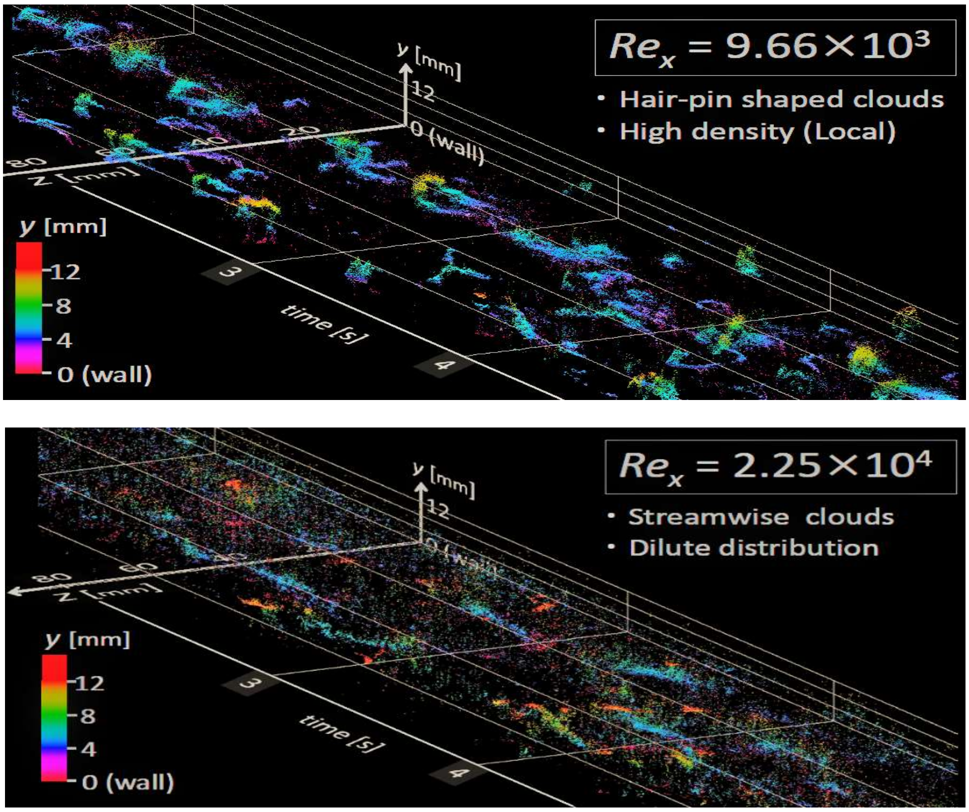

Figure 4 3-D distribution of microbubbles. (Top) Rex = 9,660 and (Bottom) Rex = 22,500.

Fig. 4 shows the three-dimensional depiction of the microbubble distribution. Here the position in y-coordinate of individual microbubble was linearly estimated from the hue value (note that the linearity was validated by our previous report (Park et al., 2019)).

3-2. Buffer layer structure

In order to assess how the liquid phase turbulence is modified by the microbubbles, we measured velocity vector of liquid phase with PIV. In parallel to the rainbow illumination for microbubbles, a laser sheet was illuminated at y = 1.0 mm from the solid wall surface in order to measure the buffer layer structure of liquid phase. Effective thickness of the laser sheet was 1.0 mm. Note that PIV measures approximately the liquid phase flow from motion of microbubbles that have no significant slip from the liquid phase. **Fig. 5** shows a sample of PIV image and its result.

After a long time-series data of PIV was obtained over 2,000 frames, we calculated several quantities that represent turbulent characteristics. **Fig. 6a** shows instantaneous wall shear stress distribution, directly computed from the streamwise velocity gradient assuming local linear shear flow within the viscous sublayer. It clearly demonstrates a spanwise stripe pattern of the wall shear stress, proving formation of low-speed streaks and high-speed sweep regions banded in an integral scale of turbulence. In the same plane, the value of u'v' was obtained as in **Fig. 6b**, which indicates the source of Reynolds shear stress. Here the velocity component perpendicular to the wall, v, was estimated from local equation of continuity integrated in the y direction. The value u'v' has a positive average value (red color) proving that it induces turbulent friction. Blue spots of negative value also appear in the plane, which means reduction of the stress due to microbubbles that are suspended in a form of clouds.

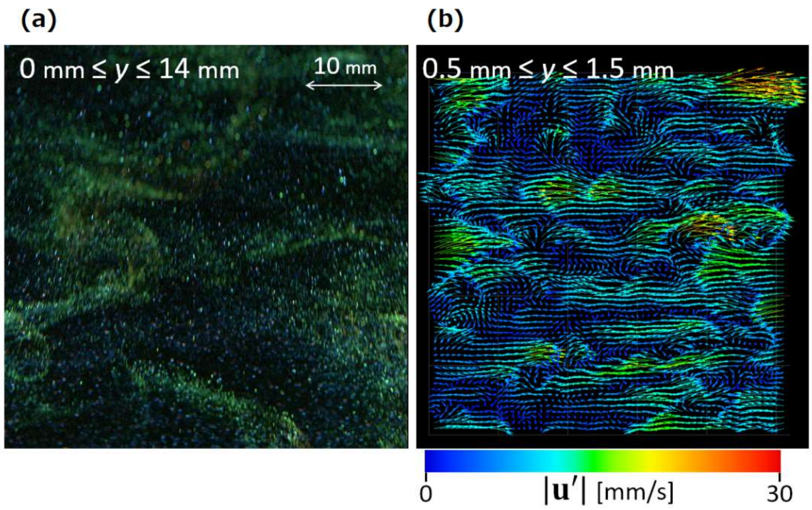

Figure 5 PIV imaging of microbubbles suspended in the buffer layer. (a) original image and (b) velocity vector obtained by PIV analysis, showing active microbubbles' sweeping correlated to Reynolds shear stress events.

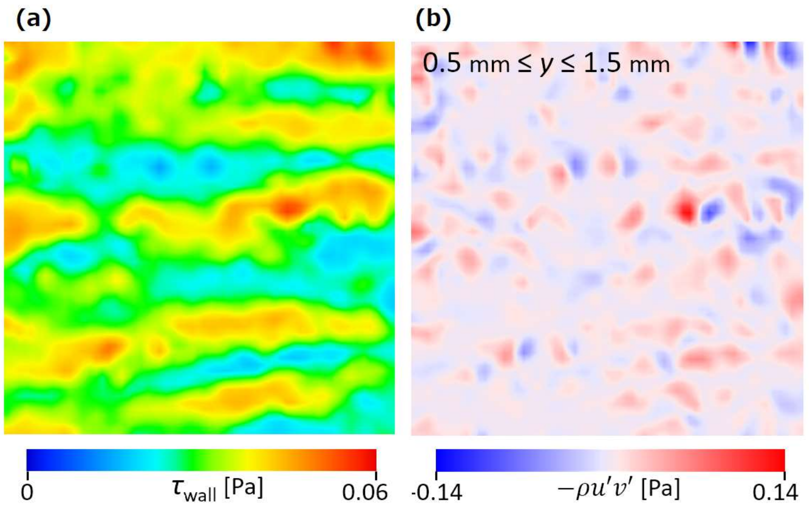

Figure 6 Instantaneous planar distribution of shear stresses. (a) The wall shear stress distribution estimated by local velocity gradient and (b) source of Reynolds shear stress estimated by computation of u′v′ distribution.

The same data of u'v' are re-visualized by **Fig. 7a**, which shows quadrant classification, i.e. Q1 (u' > 0, v' > 0), Q2 (u' < 0, v' > 0), Q3 (u' < 0, v' < 0), and Q4 (u' > 0, v' < 0). Here, Q2 and Q4 correspond to ejection and sweep, respectively. The result supports that the ejection regions (blue in the figure) are elongated in the streamwise direction having a specific spanwise interval. This is consistent to the formation of low-speed streaks in the viscous sublayer. Sweep regions (red) appear in the non-ejection regions with a local fluctuation. Since all the three velocity components, u, v, and w were measured in the present method, Q-value (second invariant quantity of velocity gradient tensor, or local Laplacian of pressure field) was also analysed as shown in **Fig. 7b**. Mostly the Q-value was obtained positively in the turbulent boundary layer, a few spots of negative value (blue region) take place. This happens unnaturally in the case of single-phase turbulent boundary layers, and hence it can be regarded as the effect of microbubble clouds. Relationship between the negative Q-value spots and the microbubble clouds is still in the stage of investigation. In our idea, there are two factors to explain the relation: one is strong viscoelasticity of the microbubble clouds, i.e, rheological effect. The other is influence of negative electric charge on the individual microbubble surface in water, which produces Coulomb force to repulse each other as microbubbles form high-number density clouds in the core of turbulent eddies.

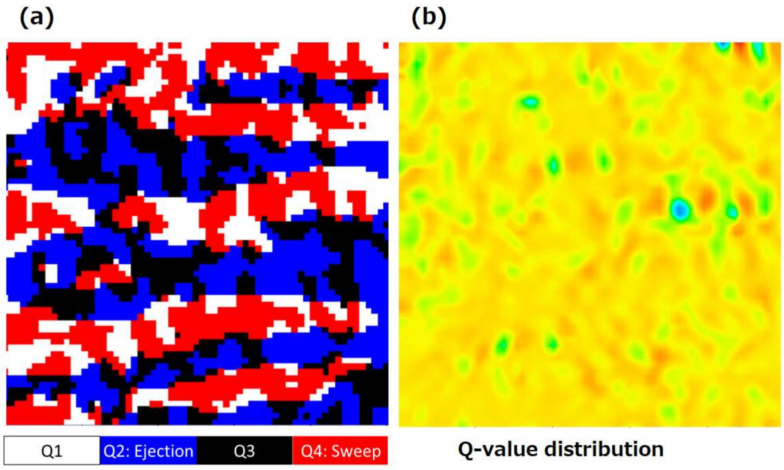

Figure 7 Visualization of the buffer layer structure altered by presence of microbubbles. (a) quadrant mapping of the component contributing to Reynolds shear stress and (b) distribution of Q-value of the velocity field.

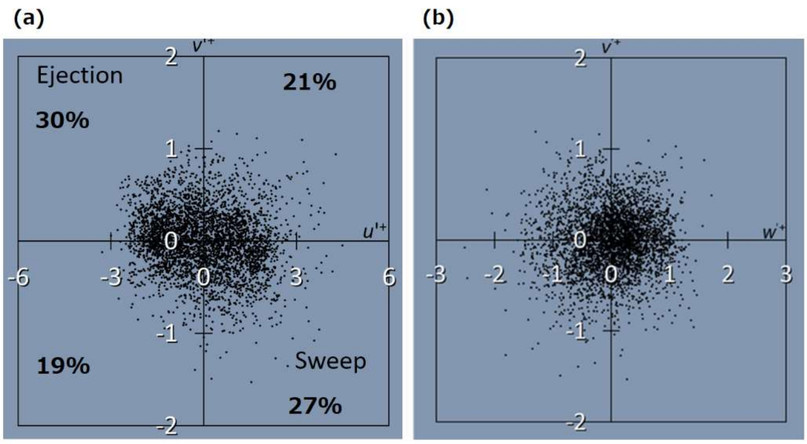

Figure 8 Correlation of velocity component fluctuations. (a) The plane of u'-v' corresponding to sweep/ejection and (b) the plane of w'-v' corresponding to spanwise symmetry

To support these ideas, we are now analysing statistic nature of the velocity correlation as shown in **Fig. 8**. In the meantime, we found that the dominancy of ejection and sweep was calmed in the case of microbubble-laden turbulent boundary layer so that turbulent frictional drag can be reduced even though the turbulent intensity itself was unchanged or rather intensified.

References

Ferrante, A., Elghobashi, S. (2004). On the physical mechanism of drag reduction in a spatially developing turbulent boundary layer laden with microbubbles. J. Fluid Mech., 503: 345–355.

Gutierrez–Torres, C. C., Hassan, Y. A., Jimenez–Bernal, J. A. (2008). Turbulence structure modification and drag reduction by microbubble injections in a boundary layer channel flow. J. Fluids Eng., 130: 111304.

Hara, K., Suzuki, T., Yamamoto, F. (2011). Image analysis applied to study on frictional drag reduction by electrolytic microbubbles in a turbulent channel flow. Exp. Fluids, 50: 715–727.

Horimoto, Y., Mori, I., Park, H. J., Tasaka, Y., Murai, Y. (2024), Bubble clustering in turbulent boundary layer on a moving wall utilizing belt-driven system. J. Fluid Sci. Tech. (in press).

Kato, H., Iwashina, T., Miyanaga, M., Yamaguchi, H. (1999). Effect of microbubbles on the structure of turbulence in a turbulent boundary layer. J. Mar. Sci. Tech., 4: 115–162

Kitagawa, A., Hishida, K., Kodama, Y. (2005). Flow structure of microbubble-laden turbulent channel flow measured by PIV combined with the shadow image technique. Exp. Fluids, 38; 466–475

Kodama, Y., Kakugawa, A., Takahashi, T., Kawashima, H. (2000). Experimental study on microbubbles and their applicability to ships for skin friction reduction. Int. J. Heat Fluid Flow, 21: 582–588.

Legner, H. H. (1984). Simple model for gas bubble drag reduction. Phys. Fluids, 27: 2788–2790.

Marie, J.L. (1987). A simple analytical formulation for microbubble drag reduction. PhysicoChemical Hydrodynamics, 8: 213–220

McCormick, M., Bhattacharyya, R. (1973). Drag reduction of a submersible hull by electrolysis. Nav. Eng. J., 85: 11–16.

Merkle, C. L., Deutsch, S. (1992). Microbubble drag reduction in liquid turbulent boundary layers. ASME Appl. Mech. Rev., 45: 103–127.

Moriguchi, Y., Kato, H. (2002). Influence of microbubble diameter and distribution on frictional resistance reduction. J. Mar. Sci. Tech., 7: 79–85.

Noto, D., Tasaka, Y., Murai, Y. (2021), In situ color-to-depth calibration: toward practical three-dimensional color particle tracking velocimetry. Exp. Fluids, 62: 131.

Noto, D., Tasaka, Y., Murai, Y. (2023), Low-cost 3D color particle tracking velocimetry: Application to thermal turbulence in water. Exp. Fluids, 64: 92.

Park H., Saito, D., Tasaka, Y., Murai, Y. (2019). Color-coded visualization of microbubbles clouds interacting with eddies in a spatially developing turbulent boundary layer, Exp. Thermal Fluid Sci., Vol. 109: 109919.

Park, H. J., Hamada, T., Kawakita, C., Murai, Y. (2023), Vertical diffusion of bubbles injected beneath a flat-bottomed ship for frictional drag reduction. Ocean Engineering, 289: 116248.

Park, H. J., Yamagishi, S., Osuka, S., Tasaka, Y., Murai, Y. (2021), Development of multi-cycle rainbow particle tracking velocimetry improved by particle defocusing technique and an example of its application on twisted Savonius turbine. Exp. Fluids, 62: 70.

Park, H., Tasaka, Y., Murai, Y. (2018). Bubbly drag reduction accompanied by void wave generation inside turbulent boundary layers, Exp. Fluids, Vol. 59: 164.

Serizawa, A., Inui, T., Eguchi, T. (2005). Flow characteristics and pseudo-laminarization of vertically upward air-water milky bubbly flow with micro bubbles in a pipe. Jpn. J. Multiphase Flow, 19: 335–340 (in Japanese).

Shatat, M. M. E., Yanase, S., Takami, T., Hyakutake, T. (2009). Drag Reduction Effects of Micro-Bubbles in Straight and Helical Pipes. J. Fluid Sci. Tech., 4: 156–167.

Tanaka, T., Oishi, Y., Park, H. J., Tasaka, Y., Murai, Y., Kawakita, C. (2022), Frictional drag reduction caused by bubble injection in a turbulent boundary layer beneath a 36-m-long flat bottom model ship. Ocean Engineering, 252: 111224.

Tanaka, T., Oishi, Y., Park, H. J., Tasaka, Y., Murai, Y., Kawakita, C. (2023), Downstream persistence of frictional drag reduction with repetitive bubble injection. Ocean Engineering, 272: 113807.

Tasaka, Y., Kimura, T., Murai, Y. (2015). Estimating the effective viscosity of bubble suspensions in oscillatory shear flows by means of ultrasonic spinning rheometry. Exp. Fluids, 56: 1867.

van Gils, D. P. M., Guzman, D. N., Sun, C., Lohse, D. (2013). The importance of bubble deformability for strong drag reduction in bubbly turbulent Taylor–Couette flow. J. Fluid Mech., 722: 317–347.

Watamura, T., Tasaka, Y., Murai, Y. (2013). Intensified and attenuated waves in a microbubble Taylor–Couette flow. Phys. Fluids, 25: 054107.

Xiong, J., Idoughi, R., Aguirre–Pablo, A. A., Aljedaani, A. B., Dun, X., Fu, Q., Thoroddsen, S. T., Heidrich, W. (2019), Rainbow particle imaging velocimetry for dense 3D fluid velocity imaging. ACM Trans. Graph., 36: 36.

Yoon, D., Park, H. J., Tasaka, Y., Murai, Y. (2022), Behaviors of sliding bubbles in an inclinable turbulent channel flow investigated by optoacoustic measurement. Int. J. Multiphase Flow, 158: 104258.